Euro. Jnl of Applied Mathematics (2008), *vol.* 19, *pp.* 191–224. © 2008 Cambridge University Press
doi:10.1017/S0956792508007353 Printed in the United Kingdom

A Survey in Mathematics for Industry
Mathematics of thermoacoustic tomography

PETER KUCHMENT[1] and LEONID KUNYANSKY[2]

[1]*Mathematics Department, Texas A&M University, College Station, TX 77843-3368, USA*
email: kuchment@math.tamu.edu
[2]*Mathematics Department, University of Arizona, Tucson, AZ 77843-3368, USA*
email: leonk@math.arizona.edu

(*Received 10 April 2007; revised 12 February 2008*)

The article presents a survey of mathematical problems, techniques and challenges arising in thermoacoustic tomography and its sibling photoacoustic tomography.

1 Introduction

Computerized tomography has had a huge impact on medical diagnostics. Numerous methods of tomographic medical imaging have been developed and are being developed (e.g., the 'standard' X-ray, single-photon emission, positron emission, ultrasound, magnetic resonance, electrical impedance, optical) [62, 67, 84–86]. The designers of these modalities strive to increase the image resolution and contrast, and at the same time to reduce the costs and negative health effects of these techniques. However, these goals are usually rather contradictory. For instance, some cheap and safe methods with good contrast (like optical or electrical impedance tomography) suffer from low resolution, while some high-resolution methods (such as ultrasound imaging) often do not provide good contrast. Recently researchers have been developing novel hybrid methods that combine different physical types of signals, in the hope of alleviating the deficiencies of each of the types, while taking advantage of their strengths. The most successful example of such a combination is the thermoacoustic tomography (TAT)[1] [69, 70, 95]. Albeit not yet a common feature in clinics, TAT scanners are actively researched, developed and already manufactured, for instance by OptoSonics, Inc. (http://www.optosonics.com/), founded by the pioneer of TAT, R. Kruger.

After a substantial effort, major breakthroughs have been achieved in the last few years in the mathematical modeling of TAT. The aim of this article is to survey this recent progress and to describe the relevant models, mathematical problems and reconstruction procedures arising in TAT and to provide references to numerous research publications on this topic.

[1]TAT is also sometimes abbreviated as TCT, which stands for thermoacoustic computed tomography. If instead of radio-frequency waves, laser beams are used to trigger the thermoacoustic signal, the procedure is called photoacoustic (PAT) or optoacoustic (OAT) tomography.

The main thrust of this text is towards mathematical methods; considerations of the text length, as well as authors' background, do not let us discuss in any detail industrial and physical set-ups and parameters of the TAT technique and limitations of the corresponding mathematical models. Fortunately, the excellent recent surveys by M. Xu and L.-H. V. Wang [131] and by A. A. Oraevsky and A. A. Karabutov [96, 97] accomplish all of these tasks, and thus the reader is advised to consult with them for all such issues (see also the recent textbook [126]). On the other hand, in spite of the significant recent progress in mathematics of TAT, there is no comprehensive survey text addressing in detail the relevant mathematical issues[2], although the surveys [97, 131] do mention some mathematical reconstruction techniques.

The structure of the article is as follows: Section 2 contains a brief description of the TAT procedure. Section 3 provides the mathematical formulation of the TAT problem. In general, it is formulated as an inverse problem for the wave equation. However, in the case of the constant sound speed, it can also be described in terms of a spherical mean operator (a spherical analogue of the Radon transform). The section also contains a list of natural questions to be addressed concerning this model. These issues are then addressed one by one in the following sections. In particular, Section 4 discusses uniqueness of reconstruction, i.e., the question of whether the data collected in TAT is sufficient for recovery of the information of interest. Although, for all practical purposes this issue is resolved in Corollary 2, we provide an additional discussion of unresolved uniqueness problems, which are probably of more academic interest. Section 5 addresses inversion formulas and algorithms. In Section 6 the effects of having only partial data are discussed. Section 7 contains results concerning the so-called range conditions, i.e., the conditions that all ideal data must satisfy. Section 8 provides additional remarks and discussions of the issues raised in the previous sections, and is followed by a bibliography. Concerning the latter, we mention that the engineering and biomedical literature on TAT is rather vast and no attempt has been made in this text to create a comprehensive bibliography of the topic from the engineering prospective. The references in [95, 96, 97, 121, 124, 131] to a large extent fill this gap. We have, however, tried to present a sufficiently complete review of the existing literature on mathematics of TAT.

2 Thermoacoustic tomography

In TAT, a short-duration electromagnetic (EM) pulse is sent through a biological object (e.g., a woman's breast in mammography) with the aim of triggering a thermoacoustic response in the tissue. As explained in [131], the radiofrequency (RF) and the visible light frequency ranges are currently considered to be the most suitable for this purpose. Since mathematics works exactly the same way in both of these frequency ranges, we will not make such a distinction and will discuss just 'an EM pulse'. For example, in Figure 1 a microwave pulse is assumed. In most cases the pulse is spatially wide, so that the whole object is more or less uniformly irradiated. Some part of EM energy is

[2]Since the submission of this article, two surveys on various topics of mathematics of TAT [41, 105] and a special issue [64] have appeared. Two other surveys [5, 40], also of a more restricted nature, are forthcoming in [125].

https://doi.org/10.1017/S0956792508007353 Published online by Cambridge University Press

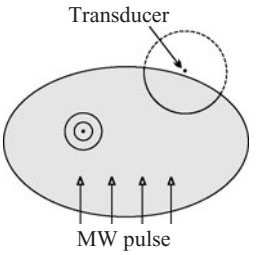

FIGURE 1. The TAT procedure.

absorbed throughout the object. The amount of energy absorbed at a location strongly depends on the local biological properties of the cells. Oxygen saturation, concentration of haemoglobin, density of the microvascular network (angiogenesis), ionic conductivity and water content are among the parameters that influence the absorption strongly [131]. Thus, if the energy absorption distribution function $f(x)$ were known, it would provide a great diagnostic tool. For instance, it could be useful for detecting cancerous cells that absorb several times more energy in the RF range than healthy ones [70, 97, 129, 131]. However, as an imaging tool neither RF waves nor visual light alone would provide acceptable resolution. In the RF case, this is due to the long wavelength. One can use shorter microwaves, but this will be at the expense of the penetration depth. In the optical region, the problem is with the multiple scattering of light. So, a different mechanism, the so-called *photoacoustic effect* [53, 119, 126, 131], is used to image $f(x)$. Namely, the EM energy absorption results in thermoelastic expansion and thus in a pressure wave $p(x, t)$ (an ultrasound signal) that can be measured by transducers placed around the object. Now one can attempt to recover the function $f(x)$ (the image) from the measured data $p(x, t)$. Such a measuring scheme, utilizing two types of waves, brings about the high resolution of the ultrasound diagnostics and the high contrast of EM waves. It overcomes the adverse effect of the low contrast of ultrasound with respect to soft tissue. In fact, such a low contrast is a good thing here, allowing one to assume in the first approximation that the sound speed is constant. This often used approximation is not always appropriate, but it is the most studied case at the moment. Later on in this text we will describe some initial considerations of the variable sound speed case, following [4, 46, 49, 65].

For this TAT method (and in particular, for the mathematical model described in the next section) to work, several conditions must be met. For instance, the time duration of the EM pulse must be shorter than the time it takes the sound wave to traverse the smallest feature that needs to be reconstructed. The ultrasound detector must be able to resolve the time scale of the duration of the EM pulse. On the other hand, the transducer must be also able to detect much lower frequencies. Thus, one needs to have extra-wide-band transducers, and these are currently available. One can find the technical discussion of all these issues, for instance, in [97, 125, 126, 131]. In this text we will assume that all these conditions are met and thus the mathematical models described are applicable.

In the next section we present a mathematical description of the relation between $f(x)$ and $p(x, t)$ (similar mathematical problems arise in sonar [81] and radar [90] imaging, as well as in geophysics [31]).

https://doi.org/10.1017/S0956792508007353 Published online by Cambridge University Press

3 Mathematical model of TAT: Wave equation and the spherical mean transform

3.1 The wave equation model

We assume that the ultrasound speed at location x is equal to $c(x)$. Then, modulo some constant coefficients that we will assume all to be equal to 1, the pressure wave $p(x,t)$ satisfies the following problem for the standard wave equation [32, 36, 119, 129]:

$$\begin{cases} p_{tt} = c^2(x)\Delta_x p, & t \geqslant 0, x \in \mathbb{R}^3 \\ p(x,0) = f(x), \\ p_t(x,0) = 0 \end{cases} \tag{3.1}$$

The goal is to find, using the data measured by transducers, the initial value $f(x)$ at $t=0$ of the solution $p(x,t)$.

In order to formalize what data is in fact measured, one needs to specify what kind of transducers are used, as well as the geometry of the measurement. By the geometry of the measurement we mean the distribution of locations of transducers used to collect the data.

We briefly describe here the commonly considered measurement procedure, which uses point detectors. Line and planar detectors have also been suggested (see Section 8.1.1). It is too early to judge which one of them will become most successful, but the one using point transducers has been more thoroughly studied mathematically and experimentally, and thus will be mostly addressed in this article. In this case, the transducers are assumed to be point-like, i.e., of sufficiently small dimension. A transducer at time t measures the average pressure over its surface at this time, which for the small size of the transducer can be assumed to be just the value of $p(y,t)$ at the location y of the transducer. Dimension count shows immediately that in order to have enough data for reconstruction of the function $f(x)$, one needs to collect data from the transducers' locations y running over a surface S in $\mathbb{R}^3$. Thus, the data at the experimentalist's disposal is the function $g(y,t)$ that coincides with the restriction of $p(x,t)$ to the set of points $y \in S$.

Taking into account that the measurements produce the values $g(y,t)$ of the pressure $p(x,t)$ of (3.1) on $S \times \mathbb{R}^+$, the set of equations (3.1) extends to become

$$\begin{cases} p_{tt} = c^2(x)\Delta_x p, & t \geqslant 0, x \in \mathbb{R}^3 \\ p(x,0) = f(x), \\ p_t(x,0) = 0 \\ p(y,t) = g(y,t), & y \in S \times \mathbb{R}^+ \end{cases} \tag{3.2}$$

The problem now reduces to finding the initial value $f(x)$ in (3.2) from the knowledge of the lateral data $g(x,t)$ (see Figure 2). A person familiar with partial differential equations might suspect first that there is something wrong with this problem, since we seem to have insufficient data for the recovery of the solution of the wave equation in a cylinder from the lateral values alone. This, however, is an illusion, since in fact there is a significant additional restriction: the solution holds in the whole space, not just inside the cylinder $S \times \mathbb{R}^+$. We will see soon that in most cases the data is sufficient for recovery of $f(x)$.

https://doi.org/10.1017/S0956792508007353 Published online by Cambridge University Press

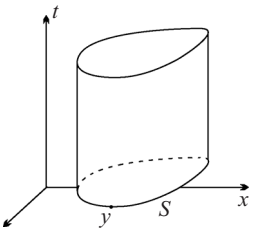

FIGURE 2. An illustration of (3.2).

3.2 Spherical mean model

We now introduce an alternative formulation of the problem that works in the constant speed case only. We will assume that the units are chosen in such a way that $c(x) = 1$. The known Poisson-Kirchhoff formula [28, Ch. VI, Section 13.2, Formula (15)] for the solution of (3.1) gives

$$p(x,t) = a\frac{\partial}{\partial t}\left(t(Rf)(x,t)\right), \tag{3.3}$$

where

$$(Rf)(x,r) = \int_{|y|=1} f(x+ry)\,dA(y) \tag{3.4}$$

is the *spherical mean operator* applied to the function $f(x)$, dA is the normalized area element on the unit sphere in $\mathbb{R}^3$ and a is a constant. Hence, knowledge of the function $g(x,t)$ for $x \in S$ and all $t \geqslant 0$ essentially means knowledge of the spherical mean $Rf(x,t)$ at all points $(x,t) \in S \times \mathbb{R}^+$. One thus is led to studying the spherical mean operator $R : f \to Rf$ and in particular its restriction R_S to the points $x \in S$ only (these are the points where we place transducers):

$$R_S f(x,t) = \int_{|y|=1} f(x+ty)dA(y), \quad x \in S, t \geqslant 0. \tag{3.5}$$

This explains why, in many works on TAT, the spherical mean operator has been the model of choice. Although the (unrestricted) spherical mean operator has been studied rather intensively and for a long time (e.g., [20, 28, 66]), its version R_S with the centres restricted to a subset S appears to have been studied only since the early 1990s [1–14, 18, 30, 34, 35, 37–41, 44, 47, 71, 72, 76, 77, 79–81, 86, 89, 91, 92, 98–100, 104, 106, 107, 116, 137] and offers quite a few new and often hard questions.

In what follows, we will alternate between these two (PDE and integral geometry) interpretations of the TAT model, since each of them has its own advantages.

3.3 Main mathematical problems of TAT

We now formulate a typical list of problems one would like to address in order to implement the TAT reconstruction.

(1) For which sets $S \in \mathbb{R}^3$ is the data collected by transducers placed along S sufficient for unique reconstruction of f? In terms of the spherical mean operator, the question

https://doi.org/10.1017/S0956792508007353 Published online by Cambridge University Press

is whether R_S has zero kernel on an appropriate class of functions, say continuous with compact support.

(2) If the data collected from S is sufficient, what are the relevant inversion formulas and algorithms?

(3) How stable is the inversion?

(4) What happens if the data is 'incomplete'?

(5) What is the space of all possible 'ideal' data $g(t, y)$ collected on a surface S? Mathematically (and in the constant sound speed case) this is the question of describing *the range* of the operator R_S in appropriate function spaces. This question might seem to be unusual (for instance, to people used to partial differential equations), but in tomography the importance of knowing the range of Radon type transforms is well known. Such information is used to improve inversion algorithms, complete incomplete data, discover and compensate for certain data errors, etc. (e.g., [34, 43–45, 60–62, 85, 86, 99, 135]).

4 Uniqueness of reconstruction

Many of the problems of interest to TAT can be formulated in any dimension d, although the practical dimensions are only $d = 3$ and $d = 2$. We will consider an arbitrary dimension d whenever appropriate.

Let $S \subset \mathbb{R}^d$ be the set of locations of the transducers and f be a compactly supported function (one can show that for purposes of uniqueness of reconstruction problem, one can always assume that f is smooth [7]). Does the absence of the signal on the transducers, i.e., $g(t, y) = 0$ for all t and y in S, imply that $f = 0$? If the answer is a 'yes,' we call S a *uniqueness set*, otherwise a *non-uniqueness set*. In other words, in terms of TAT, the uniqueness sets are those for which distributing transducers along them provides enough data for unique reconstruction of the function $f(x)$.

In terms of the wave equation, uniqueness sets are the sets of complete observability, i.e., such that observing the motion on this set only, one gets enough information to reconstruct the whole oscillation. In terms of the spherical mean operator, the question is whether the equality $R_S f = 0$ implies that $f = 0$.

We will address this problem for the constant sound speed case first.

4.1 Constant speed case

As it has been discussed, the dimension count makes it clear that S must be $(d-1)$-dimensional, i.e., a surface in 3D or a curve in 2D. We will also see that most of such surfaces are 'good', i.e., are uniqueness ones (or, in other words, provide enough information for reconstruction). Thus, we should rather discuss the problem of describing the 'bad', non-uniqueness sets. The following simple statement is very important and not immediately obvious.

Lemma 1 [7, 79, 80, 137] *Any non-uniqueness set S is a set of zeros of a (non-trivial) harmonic polynomial. In particular,*

https://doi.org/10.1017/S0956792508007353 Published online by Cambridge University Press

(1) *If there is no non-zero polynomial vanishing on S, then S is a uniqueness set.*

(2) *If there is no non-zero harmonic function vanishing on S, then S is a uniqueness set.*

The proof of this lemma is very simple. It works under the assumption of exponential decay of the function $f(x)$, not necessarily of compactness of its support. It also introduces some polynomials that play a significant role in the whole analysis of the spherical mean operator R_S.

Let $k \geqslant 0$ be an integer. Consider the convolution

$$Q_k(x) = |x|^{2k} * f(x) = \int |x-y|^{2k} f(y)\, dy. \tag{4.1}$$

This is clearly a polynomial of degree at most $2k$. Rewriting the integral in polar coordinates centered at x and using radiality of $|x-y|$, one sees that $Q_k(x)$ is determined if we know the values $Rf(x,t)$ of the spherical mean of f centered at x:

$$Q_k(x) = c_d \int_0^\infty t^{2k+d-1} Rf(x,t)\, dt.$$

In particular, if $R_S f \equiv 0$, then each polynomial Q_k vanishes on S.

Another observation that is easy to justify is that if the function f is exponentially decaying (e.g., is compactly supported), then if all polynomials Q_k vanish identically, the function itself must be equal to zero. (This is not necessarily true any more if f and its derivatives decay only faster than any power, rather than exponentially.)

Thus, we conclude that if f is not identically equal to zero, then there is at least one non-zero polynomial Q_k. Since, as we discussed, equality $R_S f = 0$ implies that $Q_k|_S = 0$, we conclude that S must be algebraic.

Now notice the following easy to verify equality (with a non-zero constant c_k):

$$\Delta Q_k = c_k Q_{k-1}, \tag{4.2}$$

where Δ is the Laplace operator. This implies that the lowest k non-zero polynomial Q_k is harmonic. Since $Q_k|_S = 0$, this proves the lemma.

Consider now the case when S is a closed (hyper-)surface (i.e., the boundary of a bounded domain). Since, as it is well known, there is no non-zero harmonic function in the domain that vanishes at the boundary (the spectrum of the Dirichlet Laplace operator is strictly positive), we conclude that such S is a uniqueness set for harmonic polynomials. Thus, we get the following important result.

Corollary 2 [7, 71] *Any closed surface is a uniqueness set for the spherical mean Radon transform.*

An older alternative proof [71] of this corollary provides an additional insight into the problem. We thus sketch it here. Let us assume for simplicity that the dimension $d \geqslant 3$ is odd (even dimensions require a little bit more work). Suppose that the closed surface S remains stationary (nodal) for the oscillation described by (3.1). Since the oscillation is unconstrained and the initial perturbation is compactly supported, after a finite time,

https://doi.org/10.1017/S0956792508007353 Published online by Cambridge University Press

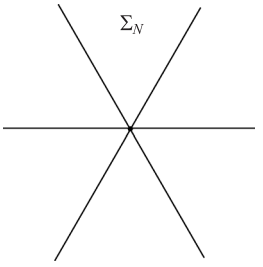

FIGURE 3. Coxeter cross Σ_N.

the interior of S will become stationary. On the other hand, we can think that S is fixed (since it is not moving anyway). Then, the energy inside S must stay constant. This is the contradiction that proves the statement of Corollary 2.

We will see in the next section that the same method works in some cases of variable sound speed, providing the needed uniqueness of the reconstruction result.

This corollary resolves the uniqueness problems for most practically used geometries. It fails, however, if f does not decay sufficiently fast (see [3], where it is shown in which $L^p(\mathbb{R}^d)$ classes of functions $f(x)$ closed surfaces remain uniqueness sets).

It also provides *uniqueness for some 'limited data' problems*. For instance, if S is an open (even tiny) piece of an analytic closed surface Σ, it suffices. Indeed, if it did not, then it would be a part of an algebraic non-uniqueness surface. Uniqueness of analytic continuation would show then that the whole Σ is a non-uniqueness set, which we know to be incorrect. This result, however, does not say that it would be practical to reconstruct using observations from a tiny S. We will see later that this would not lead to a satisfactory reconstruction, due to instabilities.

A geometry sometimes used is the planar one, i.e., detectors are placed along a plane S (line in 2D). In this case, there is no uniqueness of reconstruction when the sound speed is constant. Indeed, if $f(x)$ is odd with respect to S, then clearly all measured data $g(t, y)$ will vanish. However, it is well known [28, 66] that functions even with respect to S can be recovered. What saves the day in TAT is that the object to be imaged is located on one side of S. Then, extending $f(x)$ as an even function with respect to S, one can still recover it from the data.

Although for all practical purposes the uniqueness of reconstruction problem is essentially resolved by Corollary 2, the complete understanding of uniqueness problem has not been achieved yet. Thus, we include below some known theoretical results and open problems.

4.1.1 *Non-uniqueness sets in* $\mathbb{R}^2$

In this section we follow the results and exposition of [7, 79, 80] in discussing uniqueness sets in 2D. What are simple examples of non-uniqueness sets? As we have already mentioned, any line S (or a hyperplane in higher dimensions) is a non-uniqueness set, since any function f odd with respect to S will clearly produce no signal: $R_S f = 0$. Analogously, consider a *Coxeter system* Σ_N of N lines passing through a point and forming equal angles (see Figure 3).

https://doi.org/10.1017/S0956792508007353 Published online by Cambridge University Press

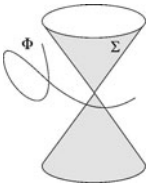

FIGURE 4. A picture of a 3D non-uniqueness set.

Choosing the intersection point as the pole and expanding functions into Fourier series with respect to the polar angle, it is easy to discover the existence of an infinite dimensional space of functions that are odd with respect to each of the N lines. Thus, such a cross Σ_N is also a non-uniqueness set. Less obviously, one can use the infinite dimensional freedom just mentioned to add any finite set Φ of points still preserving non-uniqueness. The following major and very non-trivial result was conjectured in [79, 80] and proven in [7]. It shows that there are no other bad sets S besides the ones we have just discovered.

Theorem 3 *A set $S \subset \mathbb{R}^2$ is a non-uniqueness set for the spherical mean transform in the space of compactly supported functions, if and only if*

$$S \subset \omega\Sigma_N \cup \Phi,$$

where Σ_N is a Coxeter system of lines, ω is a rigid motion of the plane and Φ is a finite set.

A sketch of a rather intricate proof of this result is provided in Section 8.2.

4.1.2 *Higher dimensions*

Here we present a believable conjecture of how the result should look in higher dimensions (see Fig. 4).

Conjecture 4 [7] *A set $S \subset \mathbb{R}^d$ is a non-uniqueness set if and only if $S \subset \omega\Sigma \cup \Phi$, where Σ is the surface of zeros of a homogeneous harmonic polynomial, ω is a rigid motion of $\mathbb{R}^d$ and Φ is an algebraic surface of dimension at most $d-2$.*

Th progress toward proving this conjecture has been slow, although some partial cases have been treated [1–12]. For example, in some cases one can prove that S is a ruled surface (i.e., consists of lines), but proving that these lines (rules) pass through a common point remains a challenge. It is known, though, that both the zero sets of homogeneous harmonic polynomials and algebraic subsets of dimension at most $d-2$ are non-uniqueness sets [2, 7], and thus one should avoid using them as placements of transducers for TAT.

4.1.3 *Relations to other areas of analysis*

The problem of injectivity of R_S has relations to a wide variety of areas of analysis (see [1, 7] for many examples). In particular, the following interpretation is important:

https://doi.org/10.1017/S0956792508007353 Published online by Cambridge University Press

Theorem 5 [7, 71] *The following statements are equivalent:*

(1) $S \subset \mathbb{R}^d$ *is a non-uniqueness set for the spherical mean operator.*

(2) S *is a nodal set for the wave equation, i.e., there exists a non-zero compactly supported* f *such that the solution of the wave propagation problem*

$$\begin{cases} \dfrac{\partial^2 u}{\partial t^2} = \Delta u, \\ u(x,0) = 0, \\ u_t(x,0) = f(x) \end{cases}$$

vanishes on S *for any moment of time.*

(3) S *is a nodal set for the heat equation, i.e., there exists a non-zero compactly supported* f *such that the solution of the problem*

$$\begin{cases} \dfrac{\partial u}{\partial t} = \Delta u, \\ u(x,0) = f(x) \end{cases}$$

vanishes on S *for any moment of time.*

The interpretation in terms of the wave equation provides important PDE tools and insights, which have led to a recent progress [12, 38] (although it has not led yet to a complete alternative proof of Theorem 3). The rough idea, originally introduced in [38], is that if S is a nodal set, then it might be considered as the fixed boundary. In this case, the signals must go around S. However, in fact, there is no obstacle, so signals can propagate along straight lines. Thus, in order to avoid discrepancies in arrival times, S must be very special. One can find details in [12] and in [38].

4.2 Uniqueness in the case of a variable sound speed

It is shown in [40, Theorem 4] that uniqueness of reconstruction also holds in the case of a smoothly varying (strictly positive) sound speed, if the source function $f(x)$ is completely surrounded by the observation surface S (in other words, if there is no ultrasound signal coming from outside of S). The proof uses the celebrated unique continuation result by D. Tataru [120].

One can also establish uniqueness of reconstruction in the case where the source is not necessarily completely surrounded by S. However, here we need to impose an additional non-trapping condition on the sound speed. We assume that the sound speed is strictly positive, $c(x) > c > 0$, and such that $c(x) - 1$ has compact support, i.e., $c(x) = 1$ for a large x.

https://doi.org/10.1017/S0956792508007353 Published online by Cambridge University Press

Consider the Hamiltonian system in $\mathbb{R}^{2n}_{x,\xi}$ with the Hamiltonian $H = \frac{c^2(x)}{2}|\xi|^2$:

$$\begin{cases} x'_t = \dfrac{\partial H}{\partial \xi} = c^2(x)\xi \\ \xi'_t = -\dfrac{\partial H}{\partial x} = -\dfrac{1}{2}\nabla\left(c^2(x)\right)|\xi|^2 \\ x|_{t=0} = x_0, \quad \xi|_{t=0} = \xi_0. \end{cases} \tag{4.3}$$

The solutions of this system are called *bicharacteristics* and their projections into $\mathbb{R}^n_x$ are *rays*.

We will assume that the following *non-trapping condition* holds: *all rays (with $\xi_0 \neq 0$) tend to infinity when $t \to \infty$.*

Theorem 6 [4] *Under the non-trapping conditions formulated above, compactly supported function $f(x)$ is uniquely determined by the data g measured on S for all times. (No assumption of f being supported inside S is imposed.)*

One should mention that ray trapping can occur for some sound speed profiles. For instance, if $c(x) = |x|$ for some range $r_1 < |x| < r_2$, then there are rays trapped in this spherical shell. We are not sure what happens in this case to the uniqueness of reconstruction statement of Theorem 6 and inversion formula of Theorem 7.

5 Reconstruction: Formulas and examples

Here we will address the procedures of actual reconstruction of the source $f(x)$ from the data $g(t, y)$ measured by transducers.

5.1 Constant sound speed

We assume here that the sound speed is constant and normalized to be equal to 1.

5.1.1 *Inversion formulas*

Before we move to our case of interest (which is spheres centered on a closed surface S surrounding the object to be imaged), we briefly refer to related but somewhat different work. Namely, the problem of recovering functions from integrals over spheres centered on a (hyper)plane S has attracted a lot of attention over the years. Although, as mentioned before, there is no uniqueness in this case (functions odd with respect to S are annihilated), even functions can be recovered. Thus also functions supported on one side of the plane can be as well, by means of their even extension. Many explicit inversion formulas and procedures have been obtained for this situation [18, 30, 35, 44, 47, 68, 86, 89, 98, 99, 111, 112, 115]. In particular, Fourier transform methods are useful here. We will not provide any details here, since this acquisition geometry does not seem very useful. In particular, this is due to 'invisibility' of some parts of the interfaces (see Section 6) which arises from truncating the plane. The same problem is encountered with some other unbounded acquisition surfaces, such as a surface of an 'infinitely' long cylinder.

https://doi.org/10.1017/S0956792508007353 Published online by Cambridge University Press

Thus, it is more practical to place transducers along a closed surface surrounding the object. The simplest surface of this type is a sphere.

5.1.2 *Fourier expansion methods*

Let us assume that S is the unit sphere in $\mathbb{R}^n$. We would like to reconstruct a function $f(x)$ supported inside S from the known values of its spherical integrals $g(y,r)$ with centres on S:

$$g(y,r) = \int_{\mathbb{S}^{n-1}} f(y + r\omega) r^{n-1}\, d\omega, \quad y \in S.$$

The first inversion procedures for the case of spherical acquisition were described in [91] in 2D and in [92] in 3D. These solutions were obtained by harmonic decomposition of the measured data and the sought function, and by equating coefficients of the corresponding Fourier series (*a la* A. Cormack's method for the X-ray CT).

In particular, the 2D algorithm of [91] is based on the Fourier decomposition of f and g in angular variables:

$$f(x) = \sum_{-\infty}^{\infty} f_k(\rho) e^{ik\varphi}, \quad x = (\rho\cos(\varphi), \rho\sin(\varphi)) \tag{5.1}$$

$$g(y(\theta), r) = \sum_{-\infty}^{\infty} g_m(r) e^{ik\theta}, \quad y = (R\cos(\theta), R\sin(\theta)).$$

Following [91] we consider the Hankel transform $\hat{g}_{m,J}(\lambda)$ of the Fourier coefficients $g_m(r)$ (divided by $2\pi r$)

$$\hat{g}_{m,J}(\lambda) = \int_0^{2R} g_m(r) J_0(\lambda r)\, dr = \mathscr{H}_0\left(\frac{g_m(r)}{2\pi r}\right). \tag{5.2}$$

To simplify the presentation we introduce the convolution $G_J(\lambda, y)$ of the sought function with the Bessel function $J_0(\lambda|x-y|)$,

$$G_J(\lambda, y) = \int_\Omega f(x) J_0(\lambda|x-y|)\, dx. \tag{5.3}$$

One can notice that $\hat{g}_{m,J}(\lambda)$ are the Fourier coefficients of $G_J(\lambda, y)$ in θ:

$$\hat{g}_{m,J}(\lambda) = \frac{1}{2\pi}\int_0^{2\pi} G_J(\lambda, y) e^{-im\theta}\, d\theta. \tag{5.4}$$

Now the coefficients $f_m(\rho)$ can be recovered from $g_m(r)$ by application of the addition theorem for the Bessel function $J_0(\lambda|x-y|)$:

$$J_0(\lambda|x-y|) = \sum_{-\infty}^{\infty} J_m(\lambda|x|) J_m(\lambda|y|) e^{-im(\varphi-\theta)}. \tag{5.5}$$

Indeed, by substituting equations (5.1) and (5.5) into (5.3), and (5.3) into (5.4) one obtains

$$\hat{g}_{m,J}(\lambda) = 2\pi J_m(\lambda|R|)\int_0^{2R} f_m(\rho) J_m(\lambda\rho)\rho\, d\rho = \mathscr{H}_m(f_m(\rho)),$$

https://doi.org/10.1017/S0956792508007353 Published online by Cambridge University Press

where $\mathscr{H}_m$ is the m-th order Hankel transform. Since the latter transform is self-invertible, the coefficients $f_m(\rho)$ can be recovered by the following formula:

$$f_m(\rho) = \mathscr{H}_m\left[\frac{\hat{g}_{m,J}(\lambda)}{J_m(\lambda|R|)}\right] = \mathscr{H}_m\left(\frac{1}{J_m(\lambda|R|)}\mathscr{H}_0\left[\frac{g_m(r)}{2\pi r}\right]\right), \tag{5.6}$$

which is the main result of [91]. The function $f(x)$ can now be reconstructed by summing series (5.1).

Note that the above method requires a division of the Hankel transform of the measured data by Bessel functions J_m that have infinitely many zeros. Theoretically, there is no problem; the Hankel transform $\mathscr{H}_0[\frac{g_m(r)}{2\pi r}]$ has to have zeros that would cancel those in the denominator. However, since the measured data always contain some error, the exact cancellation is not likely to happen, and one needs a sophisticated regularization scheme to keep the total error bounded.

This problem can be avoided by replacing in (5.2) the Bessel function J_0 by the Hankel function $H_0^{(1)}$:

$$\hat{g}_{m,H}(\lambda) = \int_0^{2R} g_m(r)H_0^{(1)}(\lambda r)\,dr.$$

The addition theorem for $H_0^{(1)}(\lambda|x-y|)$ takes the form

$$H_0^{(1)}(\lambda|x-y|) = \sum_{-\infty}^{\infty} J_m(\lambda|x|)H_m^{(1)}(\lambda|y|)e^{-im(\varphi-\theta)},$$

and by proceeding as before one can obtain the following formula for $f_m(\rho)$:

$$f_m(\rho) = \mathscr{H}_m\left[\frac{\hat{g}_{m,H}(\lambda)}{H_m^{(1)}(\lambda|R|)}\right] = \mathscr{H}_m\left(\frac{1}{H_m^{(1)}(\lambda|R|)}\int_0^{2R} g_m(r)H_0^{(1)}(\lambda r)\,dr\right).$$

Unlike J_m, Hankel functions $H_m^{(1)}(t)$ do not have zeros for any real values of t and therefore problems with division by zeros do not arise in this amended version of the method [91].

This derivation can be repeated in 3D, with the exponentials $e^{ik\theta}$ replaced by the spherical harmonics, and with cylindrical Bessel functions replaced by their spherical counterparts. By doing this one will arrive at the Fourier series method of [92]. Our use of Hankel function $H_0^{(1)}$ above is similar to the way the authors of [92] utilized spherical Hankel function $h_0^{(1)}$ to avoid the divisions by zero.

5.1.3 *Filtered backprojection methods*

The most popular way of inverting Radon transform for tomography purposes is by using filtered backprojection-type formulas, which involve filtration in Fourier domain followed (or preceded) by a backprojection. In the case of the set of spheres centred on a closed surface (e.g., a sphere) S, one expects such a formula to involve a filtration with respect to the radius variable and then some integration over the set of spheres passing through the point of interest. For quite a while, no such formula had been discovered, and even its existence had been questioned. This did not prevent practitioners from the reconstructions, since good approximate inversion formulas (parametrices) could be developed, followed

https://doi.org/10.1017/S0956792508007353 Published online by Cambridge University Press

by an iterative improvement of the reconstruction (see, e.g. the reconstruction procedures in [128, 129, 132–134], and especially [106, 107]).

The first set of exact inversion formulas of filtered backprojection type was discovered in [38]. These formulas were obtained only in odd dimensions. Several different variations of such formulas (different in terms of the exact order of the filtration and backprojection steps) were developed. Let us denote by $g(p,r) = r^2 R_S f$ the spherical integral, rather than the average, of f. Then various versions of the 3D inversion formulas that reconstruct a function $f(x)$ supported inside S from its spherical mean data $R_S f$ read

$$\begin{aligned} f(x) &= -\frac{1}{8\pi^2 R} \Delta_x \int_{\partial B} g(y, |y-x|)\, dA(y), \\ f(x) &= -\frac{1}{8\pi^2 R} \int_{\partial B} \left(\frac{d^2}{dt^2} g(y,t) \right) \Big|_{t=|y-x|} dA(y), \\ f(x) &= -\frac{1}{8\pi^2 R} \int_{\partial B} \left(\frac{d}{dt} \left(\frac{1}{t} \frac{d}{dt} \frac{g(y,t)}{t} \right) \right) \Big|_{t=|y-x|} dA(y). \end{aligned} \tag{5.7}$$

Recently, analogous formulas were obtained for even dimensions in [37]. Denoting by g, as before the spherical integrals (rather than averages) of f, the formulas of [37] in 2D look as follows:

$$f(x) = \frac{1}{2\pi R} \Delta \int_{\partial B} \int_0^{2R} g(y,t)\, \log(t^2 - |x-y|^2)\, dt\, dl(y), \tag{5.8}$$

or

$$f(x) = \frac{1}{2\pi R} \int_{\partial B} \int_0^{2R} \frac{\partial}{\partial t} \left(t \frac{\partial}{\partial t} \frac{g(y,t)}{t} \right) \log(t^2 - |x-y|^2)\, dt\, dl(y), \tag{5.9}$$

A different set of explicit inversion formulas that work in arbitrary dimensions was presented in [77]:

$$f(x) = \frac{1}{4(2\pi)^{n-1}} \operatorname{div} \int_{\partial B} \mathbf{n}(y) h(y, |x-y|)\, dA(y). \tag{5.10}$$

Here

$$\begin{aligned} h(y,t) = \int_{\mathbb{R}^+} \Bigg[& Y(\lambda t) \left(\int_0^{2R} J(\lambda t') g(y,t')\, dt' \right) \\ & - J(\lambda t) \left(\int_0^{2R} Y(\lambda t') g(y,t')\, dt' \right) \Bigg] \lambda^{2n-3}\, d\lambda, \end{aligned} \tag{5.11}$$

$$J(t) = \frac{J_{n/2-1}(t)}{t^{n/2-1}}, \quad Y(t) = \frac{Y_{n/2-1}(t)}{t^{n/2-1}},$$

$J_{n/2-1}(t)$ and $Y_{n/2-1}(t)$ are respectively the Bessel and Neumann functions of order $n/2-1$, and $\mathbf{n}(y)$ is the vector of exterior normal to ∂B.

In 2D equations (5.10), (5.11) can be simplified to yield the following reconstruction formula:

$$f(x) = -\frac{1}{2\pi^2} \operatorname{div} \int_{\partial B} \mathbf{n}(y) \left[\int_0^{2R} g(y,t') \frac{1}{|x-y|^2 - t'^2}\, dt' \right] dl(y).$$

https://doi.org/10.1017/S0956792508007353 Published online by Cambridge University Press

A similar simplification is also possible in 3D resulting in the formula

$$f(x) = \frac{1}{8\pi^2}\mathrm{div}\int_{\partial B}\mathbf{n}(y)\left(\frac{1}{t}\frac{d}{dt}\frac{g(y,t)}{t}\right)\Bigg|_{t=|y-x|} dA(y). \tag{5.12}$$

Equation (5.12) is equivalent to one of the formulas derived in [130] for the 3D case. It is interesting to notice that the 'universal' formula of [130] holds for all geometries when the backprojection-type formulas are known: spherical, cylindrical and planar. It is not very likely that such explicit formulas would be available for any closed surfaces S different from spheres (see a related discussion in [15, 31]).

5.1.4 *Series solutions for arbitrary geometries*

Although, as we have just mentioned, we do not expect such explicit formulas to be derived for non-spherical closed surfaces S, there is, however, a different approach [78] that theoretically works for any closed S and that is practically useful in some non-spherical geometries.

Let λ_m^2 and $u_m(x)$ be the eigenvalues and normalized eigenfunctions of the Dirichlet Laplacian $-\Delta$ on the interior Ω of a closed surface S:

$$\begin{aligned} \Delta u_m(x) + \lambda_m^2 u_m(x) &= 0, \quad x \in \Omega, \quad \Omega \subseteq \mathbb{R}^n, \\ u_m(x) &= 0, \quad x \in S, \\ ||u_m||_2^2 &\equiv \int_\Omega |u_m(x)|^2\, dx = 1. \end{aligned} \tag{5.13}$$

As before, we would like to reconstruct a compactly supported function $f(x)$ from the known values of its spherical integrals $g(y,r)$ with centres on S:

$$g(y,r) = \int_{\omega^{n-1}} f(y + r\omega) r^{n-1}\, d\omega, \quad y \in S.$$

We notice that $u_m(x)$ is the solution of the Dirichlet problem for the Helmholtz equation with zero boundary conditions and the wave number λ_m, and thus it admits the Helmholtz representation

$$u_m(x) = \int_{\partial\Omega} \Phi_{\lambda_m}(|x-y|)\frac{\partial}{\partial\mathbf{n}}u_m(y)\, ds(y), \quad x \in \Omega, \tag{5.14}$$

where $\Phi_{\lambda_m}(|x-y|)$ is a free-space rotationally invariant Green's function of the Helmholtz equation (5.13).

The eigenfunctions $\{u_m(x)\}_0^\infty$ form an orthonormal basis in $L_2(\Omega)$. Therefore, $f(x)$ can be represented by the series

$$f(x) = \sum_{m=0}^{\infty} \alpha_m u_m(x) \tag{5.15}$$

with

$$\alpha_m = \int_\Omega u_m(x) f(x)\, dx.$$

https://doi.org/10.1017/S0956792508007353 Published online by Cambridge University Press

Since $f(x) \in C_0^1$, series (5.15) converges pointwise. A reconstruction formula of α_m, and thus of $f(x)$, will result if we substitute representation (5.14) into (5.15) and interchange the order of integration. Indeed, after a brief calculation we will get

$$\alpha_m = \int_\Omega u_m(x) f(x)\, dx = \int_{\partial\Omega} I(y, \lambda_m) \frac{\partial}{\partial \mathbf{n}} u_m(y)\, dA(x), \tag{5.16}$$

where

$$I(y, \lambda) = \int_\Omega \Phi_\lambda(|x - y|) f(x)\, dx. \tag{5.17}$$

Certainly, the need to know the spectrum and eigenfunctions of the Dirichlet Laplacian imposes a severe constraint on the surface S. However, there are simple cases when the eigenfunctions are well known, and fast summation formulas for the corresponding series are available. Such is the case of a cubic measuring surface S (see [78]); the eigenfunctions u_m are products of sine functions:

$$u_m(x) = \frac{8}{R^3} \sin\frac{\pi m_1 x_1}{R} \sin\frac{\pi m_2 x_2}{R} \sin\frac{\pi m_3 x_3}{R}, \tag{5.18}$$

where $m = (m_1, m_2, m_3)$, $m_1, m_2, m_3 \in \mathbb{N}$, and the eigenvalues are easily found as well:

$$\lambda_m = \pi^2 |m|^2 / R^2. \tag{5.19}$$

Sum (5.15) is just a regular 3D Fourier sine series easily computable by application of the Fast Fourier Sine transform algorithm. The algorithmic trick that allows one to calculate the coefficients α_m quickly consists in first computing integrals (5.17) on a uniform mesh in λ. This is easily done by a 1D Fast Fourier Cosine transform algorithm, with $\Phi_\lambda(t) = \cos(\lambda t)/t$. The normal derivatives of $u_m(x)$ are also products of sine functions, this time 2D ones. This, in turn, permits rapid evaluation of the integrals $\int_{\partial\Omega_i} I(y, \lambda) \frac{\partial}{\partial \mathbf{n}} u_m(y)\, dA(x)$ for each mesh value of λ, and for each one of the six faces $\partial\Omega_i, i = 1, \ldots, 6$, of the cube. Finally, the computation of α_m using equation (5.16) reduces to the interpolation in the spectral parameter λ, since the integrals in the right-hand side of this equation have been computed for the mesh values of this parameter (not for λ_m). Due to the oscillatory nature of the integrals (5.17) a low-order interpolation here would lead to inaccurate reconstructions. Luckily, however, these integrals are analytic functions of the parameter λ (due to the finite support of g). Hence, high-order polynomial interpolation is applicable, and numerics yields very good results.

The algorithm we just described requires $\mathcal{O}(m^3 \log m)$ floating point operations if the reconstruction is to be performed on an $m \times m \times m$ Cartesian grid, from comparably discretized data measured on a cubic surface. In practical terms, it yields reconstructions in the matter of several seconds on grids with total number of nods exceeding a million [78].

5.1.5 *Time reversal (backpropagation) methods*

In the constant speed case, the following approach is possible in 3D [38]: due to the validity of the Huygens' principle (i.e., the signal escapes from any bounded domain in finite time), the pressure $p(t, x)$ inside S will become equal to zero for any time T larger

https://doi.org/10.1017/S0956792508007353 Published online by Cambridge University Press

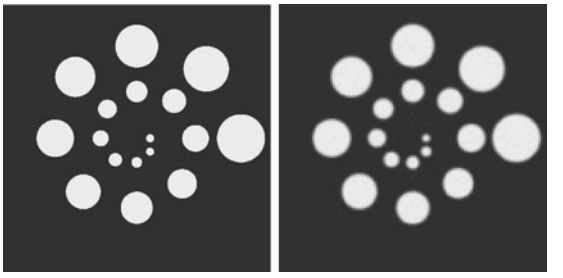

FIGURE 5. A mathematical phantom in 3D (left) and its reconstruction using an analytic inversion formula.

than the time required to cross the domain (i.e., time that it takes the sound to move along the diameter of S, which for $c = 1$ equals the diameter). Thus, one can impose zero conditions on $p(t, x)$ for $t = T$ and solve the wave equation (3.2) back in time, using the measured data g as the boundary values. The solution of this well-posed problem at $t = 0$ gives the desired source function $f(x)$. Such methods have been successfully implemented [25].

Although in 2D or in presence of sound speed variations Huygens' principle does not hold any more, and thus the signal theoretically will stay forever, one can find good approximate solutions using a similar approach [4, 46, 49]; see discussions of the variable speed case later.

5.1.6 *Examples of reconstructions and additional remarks about the inversion formulas*

It is worth noting that although formulas (5.7)–(5.8) and (5.10)–(5.12) will yield identical results when applied to functions that can be represented as the spherical mean Radon transform of a function supported inside S, they are in general not equivalent when applied to functions with larger supports. Simple examples (e.g., of f being the characteristic set of a large ball containing S) show that these two types of formulas provide different reconstructions. They also are not equivalent on data that contain errors.

It is well known that different analytic inversion formulas in tomography can behave differently in numerical implementation (e.g., in terms of their stability). However, numerical implementation seems to show that the analytic (backprojection type) formulas (5.7)–(5.12), in spite of them being not equivalent on data that involve errors, work equally well. See, for example, the results of an analytic formula reconstruction in 3D shown in Figure 5.

An interesting observation is that backprojection formulas (5.7)–(5.12) do not reconstruct the function f correctly inside the surface S, if f has support reaching outside S. For instance, applying the reconstruction formulas to the function $R_S(\chi_{|x|\leqslant 3})$ leads to an incorrect reconstruction of the value of $f = \chi_{|x|\leqslant 3}$ inside $S = \{|x| \leqslant 1\}$. (Here by χ_V we denote the characteristic function of the set V, i.e., it takes the value 1 in V and zero

https://doi.org/10.1017/S0956792508007353 Published online by Cambridge University Press

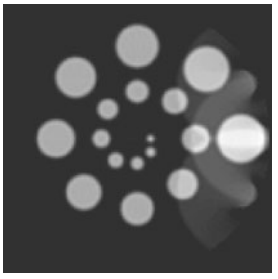

FIGURE 6. A perturbed reconstruction due to presence of two additional balls outside S (not shown in the picture).

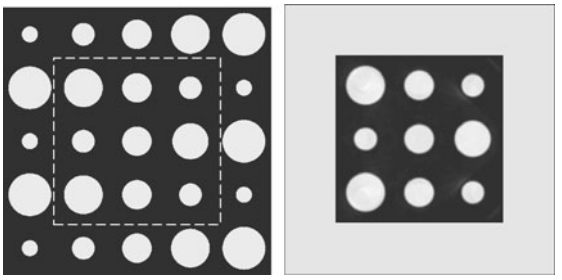

FIGURE 7. In the phantom shown on the left, most disks are located outside the square acquisition surface S indicated by the dotted line. This does not perturb the reconstruction inside S (right).

outside. So, $\chi_{|x|\leqslant 3}$ is the characteristic function of the ball of radius 3 centered at the origin.)

As another example, if one adds to the phantom shown in Figure 5 two balls to the right of the surrounding sphere S, this leads to strong artifacts, as seen in Figure 6.

What is the reason for such a distortion? If one does not know in advance that f has support inside S, the backprojection formulas shown before use insufficient information to recover a function with a larger support, and thus uniqueness of reconstruction is lost. Then the formulas misinterpret the data, wrongly assuming that they came from a function supported inside S and thus reconstructing the function incorrectly. The backprojection formulas make significant use of the assumption of f being supported inside S and also of the time derivative of the pressure vanishing at time $t = 0$. It is not clear whether such formulas are possible without these assumptions.

Notice that the series reconstruction of the preceding section is free of such problem. For example, the reconstruction shown in Figure 7 confirms this.

The reason of such robustness of the series reconstructions is that the only assumption they use is a sufficiently fast decay of the solution (pressure) inside S. This condition holds, for instance, when f has a compact support (not necessarily surrounded by the observation surface S) and when the sound speed satisfies a non-trapping condition (see the next section), e.g., is constant. See [46] for this discussion.

https://doi.org/10.1017/S0956792508007353 Published online by Cambridge University Press

5.2 Reconstruction in the variable speed case

We will assume here that the sound speed $c(x)$ is smooth, positive, constant for a large x and non-trapping. Although most analytic techniques we described above do not work in the variable speed case, some formulas can be derived and algorithms can be designed. This work is at an early stage and the results described hereafter most surely can and will be improved.

5.2.1 *'Analytic' inversions*

Let us denote by Ω the interior of the observation surface S, i.e., the area where the object to be imaged is located. Consider in Ω the operator $A = -c^2(x)\Delta$ with zero Dirichlet conditions on the boundary $S = \partial\Omega$. This operator is self-adjoint, if considered in the weighted space $L^2(\Omega; c^{-2}(x))$.

We also denote by E the operator of harmonic extension, which transforms a function ϕ on S to a harmonic function on Ω which coincides with ϕ on S.

The following result provides a formula for reconstructing f from the data g:

Theorem 7 [4] *The function $f(x)$ in (3.2) can be reconstructed in Ω as follows:*

$$f(x) = (Eg|_{t=0}) - \int_0^\infty A^{-\frac{1}{2}} \sin(\tau A^{\frac{1}{2}}) E(g_{tt})(x,\tau)\, d\tau. \tag{5.20}$$

The validity of this result hinges upon decay estimates for the solution (so-called local energy decay [33, 122, 123]), which hold under the non-trapping condition. These estimates guarantee a qualified decay of the solution $p(t,x)$ inside any bounded region, e.g., in Ω, when time t increases. In odd dimensions decay is exponential, but only polynomial in even dimensions. The decay can be used instead of Huygens' principle to solve the wave equation backwards, starting at infinite time. This leads to the formula (5.20).

Due to functions of the operator A being involved, it is not that clear how explicit and practical this formula can be made. For instance, it would be interesting to see whether one can derive from (5.20) a backprojection inversion formula for the case of a constant sound speed and S being a sphere (we have already seen that such formulas are known).

5.2.2 *Backpropagation*

The decay at large values of time can be used as follows: for a sufficiently large T, one can assume that the solution is practically zero at $t = T$. Thus, imposing zero initial conditions at $t = T$ and solving in the reverse time direction, one arrives at $t = 0$ to an approximation of $f(x)$. Numerical experiments [46, 49] show that this works even under worst of circumstances, in 2D and with a trapping sound speed.

5.2.3 *Eigenfunction expansions*

One natural way to try to use the formula (5.20) is to use the eigenfunction expansion of the operator A in Ω (assuming that such expansion is known). This immediately leads to the following result:

https://doi.org/10.1017/S0956792508007353 Published online by Cambridge University Press

Theorem 8 *Under the same conditions on the sound speed as before, function $f(x)$ can be reconstructed inside Ω from the data g in (3.2), as the following $L^2(B)$-convergent series:*

$$f(x) = \sum_k f_k \psi_k(x), \tag{5.21}$$

where the Fourier coefficients f_k can be recovered using one of the following formulas:

$$\begin{aligned} f_k &= \lambda_k^{-2} g_k(0) - \lambda_k^{-3} \int_0^\infty \sin(\lambda_k t) g_k''(t)\, dt, \\ f_k &= \lambda_k^{-2} g_k(0) + \lambda_k^{-2} \int_0^\infty \cos(\lambda_k t) g_k'(t)\, dt, \ \textit{or} \\ f_k &= -\lambda_k^{-1} \int_0^\infty \sin(\lambda_k t) g_k(t)\, dt = -\lambda_k^{-1} \int_0^\infty \int_S \sin(\lambda_k t) g(x,t) \overline{\frac{\partial \psi_k}{\partial \nu}(x)}\, dx\, dt, \end{aligned} \tag{5.22}$$

and

$$g_k(t) = \int_S g(x,t) \overline{\frac{\partial \psi_k}{\partial \nu}(x)}\, dx.$$

Here ν denotes the external normal to S.

One notices that this is a generalization to the variable sound speed case of the expansion method of [78], discussed in Section 5.1.4. An interesting feature is that, unlike in [78], we do not need to know the whole space Green's function for A (which is certainly not known). However, it is not clear yet how feasible numerical implementation of this approach could be.

6 Partial data: 'Visible' and 'invisible' singularities

Uniqueness of reconstruction does not imply practical recoverability, since the reconstruction procedure might be severely unstable. This is well known to be the case, for instance, in incomplete data situations in X-ray tomography, and even for complete data problems in some imaging modalities, such as the electrical impedance tomography [72, 76, 85, 86].

In order to describe the results below, we need to explain the notion of the wave front set $WF(f)$ of a function $f(x)$. This set carries detailed information on singularities of $f(x)$. It consists of pairs (x, ξ) of a point x in space and a wave vector (Fourier domain variable) $\xi \neq 0$. It is easier to say what it means that a point (x_0, ξ_0) is *not in* the wave front set $WF(f)$. This means that one can smoothly cut off f to zero at a small distance from x_0 in such a way that the Fourier transform $\widehat{\phi f}(\xi)$ of the resulting function $\phi(x) f(x)$ decays faster than any power of ξ in directions that are close to the direction of ξ_0. We remind the reader that if this Fourier transform decays that way in *all* directions, then $f(x)$ is smooth near the point x_0. So, the wave front set consists of pairs (x_0, ξ_0) such that f is not smooth near x_0, and ξ_o indicates why it is not: the Fourier transform does not decay well in this direction. For instance, if $f(x)$ consists of two smooth pieces joined non-smoothly across a smooth interface Σ, then $WF(f)$ contains pairs (x, ξ) such that x is in Σ and ξ is normal to Σ at x. One can find simple introduction to the notions of microlocal analysis, such as the wave front set, for instance in [118].

https://doi.org/10.1017/S0956792508007353 Published online by Cambridge University Press

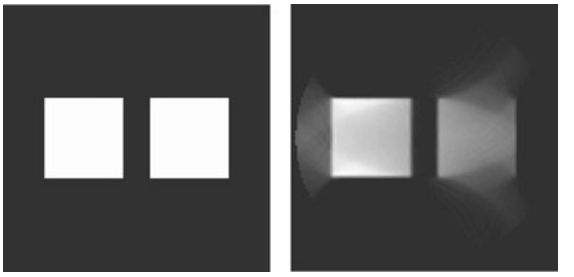

FIGURE 8. Effect of incomplete data: the phantom (left) and its incomplete data reconstruction. The transducers were located along a 180° circular arc (the left half of a large circle surrounding the squares).

Analysis done in [109] for the Radon transform case[3] showed which parts of the wave front (and thus singularities) of a function f can be recovered from its partial X-ray data. An analogue of this result also holds for the spherical mean transform R_S [81] (see also [134, 135] for a practical discussion). We formulate it below in an imprecise form (see [81] for precise formulation).

Theorem 9 [81] *A wave front set point (x, ξ) of f is 'invisible' (i.e., is not stably recoverable from $R_S f$), unless there is a circle (sphere in higher dimensions) centred on the observation surface S, passing through x, and normal to ξ at this point.*

As we have already mentioned, this result does not exactly hold the way it is formulated and needs to include some precise conditions (see [81, Theorem 3]). The statement is, for instance, correct if S is a smooth hypersurface and the support of f lies on one side of the tangent plane to S at the center of the sphere mentioned in the theorem.

Talking about jump singularities only (i.e., interfaces between smooth regions inside the object to be imaged), this result says that in order for a piece of the interface to be stably recoverable (dubbed 'visible'), one should have for each point of this interface a sphere centered at S and tangent to the interface at this point. In other words, if at a point x of an interface L there is no detector located along the normal line to L at this point, this part of the interface will be mandatorily blurred in the reconstructed image. The reason is that if all spheres of integration are transversal to the interface, the integration smooths off the singularity, and therefore its recovery becomes highly unstable. Numerically, one has to deal with inversion of a matrix with exponentially fast decaying singular values, or with filtration with a filter that grows super-polynomially with the frequency. Figure 8 shows an example of an incomplete data reconstruction from spherical mean data. One sees clearly the effect of disappearance of the parts of the boundaries that are not touched tangentially by circles centred at transducers' locations. A useful notion is the one of a *detection region*, i.e., the region where for any point x any line passing through x also passes through a detector location. For instance, if S is a spherical cap, the detection region will be the convex hull of the cup (if S is a half-sphere, the detection region is the corresponding half-ball). If the object f to be imaged is contained entirely inside the

[3] See a somewhat more limited related result in [113].

https://doi.org/10.1017/S0956792508007353 Published online by Cambridge University Press

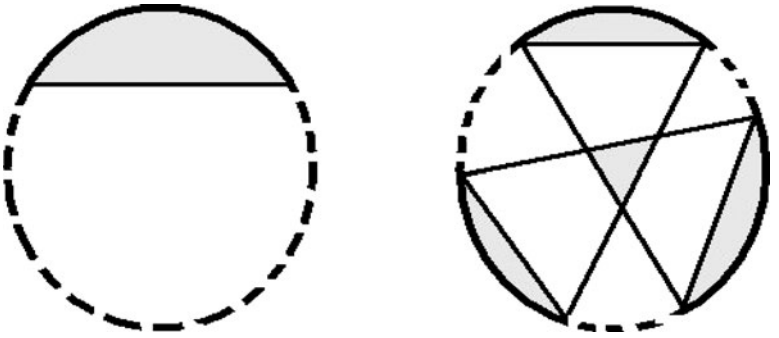

FIGURE 9. The arcs where the detectors are located are shown with solid line. Dotted lines indicate the locations where detectors are not being placed. The shaded regions are the detection domains.

detection region, there will be no blurring of its singularities, and in fact the object can be stably imaged. Figure 9 shows the 2D detection regions (shaded) when S is a single arc of a circle and when it is the union of three arcs.

One should mention that the blurring due to 'invisibility' cannot be overcome, no matter which inversion algorithm is used, unless some additional information about the object is known and incorporated (as, for instance, in [127]), or the physical set-up of the measurements is changed (e.g., in [29] mirrors are used to reflect back to the transducers the waves that would have been otherwise unaccounted for).

The half-sphere problem, important for breast imaging, has in particular attracted a lot of attention. Even if the object is inside the detection region (half-ball), the reconstructions, although not suffering from blurring, show deterioration in intensity of the image. Various partial solutions have been suggested: better approximate inverses, corrective coefficients, numerical minimization, using range conditions for recovering the missing data, etc. (e.g., [16, 17, 19, 104]). A recent work in progress (L. Kunyansky, personal communication, January 2008) shows promise for good reconstructions in this case.

7 Range conditions

As already mentioned, the space of functions $g(t, y)$ that could arise as exact data measured by transducers (i.e., the range of the data) is very small (of infinite codimension in the spaces of all functions of $t > 0, y \in S$). Knowing this space (range) is useful for many theoretical and practical purposes (reconstruction algorithms, error corrections, incomplete data completion, etc.), and thus has attracted a lot of attention (e.g., [34, 43–45, 60, 61, 72, 74–76, 82, 85–87, 99, 110].

For instance, for the standard Radon transform

$$f(x) \to g(s, \omega) = \int_{x \cdot \omega = s} f(x)\, dx, |\omega| = 1,$$

the range conditions on $g(s, \omega)$ are

(1) *evenness*: $g(-s, -\omega) = g(s, \omega)$

https://doi.org/10.1017/S0956792508007353 Published online by Cambridge University Press

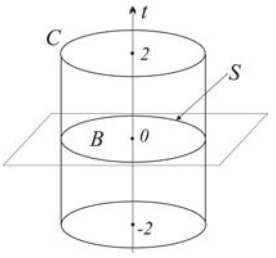

FIGURE 10. An illustration to Theorem 10.

(2) *moment conditions*: for any integer $k \geqslant 0$, the kth moment

$$G_k(\omega) = \int_{-\infty}^{\infty} s^k g(\omega, s)\, ds$$

extends from the unit circle of vectors ω to a homogeneous polynomial of degree k in ω.

The evenness condition is obviously necessary and is kind of 'trivial'. It seems that the only non-trivial conditions are the moment ones. However, here the standard Radon transform misleads us, as it often happens. In fact, for more general transforms of Radon type it is often easy (or easier) to find analogues of the moment conditions, while analogues of the evenness conditions are often elusive (see [72, 74, 75, 85, 86, 93] devoted to the case of SPECT (single-photon emission tomography)). The same happens in TAT.

Let us deal first with the case of a constant sound speed, when one can think of the spherical mean transform R_S instead of the wave equation model. An analogue of the moment conditions was already present implicitly (without saying that these were range conditions) in [7, 79, 80] and explicitly formulated as such in [104]. Indeed, our discussion in Section 4 of the polynomials Q_k provides the following conditions of moment type:

Moment conditions [7, 79, 80, 104] *on data* $g(p,r) = R_S f(p,r)$ *look as follows: for any integer* $k \geqslant 0$, *the moment*

$$M_k(\omega) = \int_0^{\infty} r^{2k+d-1} g(p,r)\, dr$$

can be extended from S *to a (non-homogeneous) polynomial* $Q_k(x)$ *of degree at most* $2k$.

These conditions, however, are incomplete, and in fact infinitely many others, which play the role of an analogue of evenness, need to be added.

Complete range descriptions for R_S when S is a circle in 2D were discovered in [13] and then in odd dimensions in [39]. They were then extended to any dimension and interpreted in several different ways in [6]. These conditions happen to be intimately related to PDEs and spectral theory.

In order to describe these conditions, we need to introduce some notation. Let B be the unit ball in $\mathbb{R}^d$, S the unit sphere and C the cylinder $B \times [0,2]$ (see Figure 10).

https://doi.org/10.1017/S0956792508007353 Published online by Cambridge University Press

We introduce the spherical mean operator R_S as before:

$$R_S f(x,t) = \int_{|y|=1} f(x+ty)\, dA(y), x \in S.$$

Several different range descriptions for R_S were provided in [6], out of which we only show a few.

Theorem 10 [6] *The following three statements are equivalent:*

(1) *The function $g \in C_0^\infty(S \times [0,2])$ is representable as $R_S f$ for some $f \in C_0^\infty(B)$. (In other words, g represents an ideal (free of errors) set of TAT data.)*

(2) (a) *The moment conditions are satisfied.*

(b) *Let $-\lambda^2$ be any eigenvalue of the Laplace operator in B with zero Dirichlet conditions and ψ_λ be the corresponding eigenfunction. Then the following orthogonality condition is satisfied:*

$$\int_{S\times[0,2]} g(x,t)\partial_\nu \psi_\lambda(x) j_{n/2-1}(\lambda t) t^{n-1}\, dx\, dt = 0. \tag{7.1}$$

Here $j_p(z) = c_p \frac{J_p(z)}{z^p}$ is the so-called spherical Bessel function.

(3) (a) *The moment conditions are satisfied.*

(b) *Let $\widehat{g}(x,\lambda) = \int g(x,t) j_{n/2-1}(\lambda t) t^{n-1}\, dt$. Then, for any $m \in \mathbb{Z}$, the m-th spherical harmonic term $\widehat{g}_m(x,\lambda)$ of $\widehat{g}(x,\lambda)$ vanishes at all zeros $\lambda \neq 0$ of the Bessel function $J_{m+n/2-1}(\lambda)$.*

Remark 11 [6]

(1) In odd dimensions, moment conditions are not necessary, and thus conditions 2(b) or 3(b) suffice. (A similar earlier result was established for a related transform in [39].)

(2) The range conditions (2) of the previous theorem are also necessary when S is the boundary of any bounded domain, not necessarily a sphere.

(3) An analogue of these conditions can be derived for a variable sound speed (without non-trapping conditions imposed).

8 Concluding remarks

8.1 Variations of the TAT procedure

8.1.1 *Planar and linear transducers*

Assuming that transducers are point-like is clearly an approximation, and in fact a transducer measures the average pressure over its area. It has been rightfully claimed that the point approximation for transducers should lead to some blurring in the reconstructions. This, as well as intricacies of reconstructions from the data obtained by point transducers,

https://doi.org/10.1017/S0956792508007353 Published online by Cambridge University Press

triggered recent proposals for different types of transducers (see [23, 24, 54–59, 101, 102]). In these papers, it was suggested to use either planar or line detectors.

In the first case [55], the detectors are assumed to be large and planar, ideally assumed to be approximations of infinite planes that are placed tangentially to a sphere containing the object. Thus, the data one collects is the integrals of the pressure over these planes, for all values of $t > 0$. If one takes the standard 3D Radon transform of the pressure $p(x, t)$ with respect to x:

$$P(x, t) \mapsto q(s, t, \omega) = \int_{x \cdot \omega = s} p(x, t)\, dA(x),$$

where dA is the surface measure and ω is a unit vector in $\mathbb{R}^3$, this is well known to reduce the 3D Laplace operator Δ_x to the second derivative $\partial^2/\partial s^2$ [34, 43–45, 60, 61], and thus the 3D wave equation to the string vibration problem. The measured data provide the boundary conditions for this problem. The initial conditions in (3.1) mean evenness with respect to time, and thus the standard d'Alambert formula leads to the immediate realization that the measured data is just the 3D Radon transform of $f(x)$. Thus, the reconstruction boils down to the well-known inversion formulas for the Radon transform.

Another proposal [23, 24, 54, 56, 57, 101, 102] is to use line detectors that provide line integrals of the pressure $p(x, t)$. Such detectors can be implemented optically, using either Fabry-Perot [24], or Mach-Zehnder [102] interferometers.

Suppose that the object is surrounded by a surface that is rotation-invariant with respect to the z-axis. It is suggested to place the line detectors perpendicular to the z-axis and tangential to the surface. The same consideration as above then shows that after the 2D Radon (or X-ray, which in 2D is the same) transform in each plane orthogonal to z-axis, the 3D wave equation converts into the 2D one for the Radon data. The measurements provide the boundary data. Thus, the reconstruction boils down to solving a 2D problem similar to the one in the case of point detectors, and then inverting the 2D Radon transform.

Due to the recent nature of these two projects, it appears to be too early to judge which one will be superior in the end. For instance, it is not clear beforehand, whether the approximation of infinite size (length, area) of the linear or planar detectors works better than the zero dimension approximation for point detectors. Further developments will resolve these questions, but probably each type of the detectors will find its niche.

8.1.2 *Direct imaging techniques*

Some direct imaging techniques have been suggested, which might not require mathematical reconstructions. See, for instance, [88] about an acoustic lens system.

8.1.3 *Using contrast agents*

Contrast agents to improve TAT imaging have been developed (e.g., [27]).

https://doi.org/10.1017/S0956792508007353 Published online by Cambridge University Press

8.1.4 *Passive thermoacoustic imaging*

The TAT model we have considered can be called 'active thermoacoustic tomography', due to the set-up when the practitioner creates the signal. There has been some recent development of the 'passive thermoacoustic tomography', where the thermoacoustic signal is used to image the temperature sources present inside the body. One can find a survey of this area in [103].

8.2 Uniqueness

8.2.1 *Sketch of the proof of Theorem 10*

We provide here a brief outline of the rather technical proof of Theorem 10.

Suppose that f is compactly supported, not identically zero, and such that $R_S f = 0$. Our previous considerations show that one can assume that S is an algebraic curve (not a straight line) that is contained in the set of zeros of a non-trivial harmonic polynomial. Now one touches the boundary of the support of f from outside by a circle centered on S. Then microlocal analysis of the operator R_S (which happens to be an analytic Fourier Integral Operator (FIO) [21, 48, 50–52, 73, 108]) shows that, due to the equality $R_S f = 0$, at the tangency point the vector co-normal to the sphere should not belong to the analytic wave front of f (microlocal regularity of solutions of $R_S f = 0$). This, for instance, can be extracted from the results of [117]. On the other hand, a theorem by Hörmander and Kashiwara [63, Theorem 8.5.6] shows that this vector must be in the analytic wave front set, since $f = 0$ on one side of the sphere (a microlocal version of uniqueness of analytic continuation). This way, one gets a contradiction. Unfortunately, the life is not so easy, and the proof sketched above does not go through smoothly, due to possible cancellation of wave fronts at different tangency points. Then one has to involve the geometry of zeros of harmonic polynomials [42] to exclude the possibility of such a cancellation.

Thus, the proof uses microlocal analysis and geometry of zeros of harmonic polynomials. Both these tools have their limitations. For instance, the microlocal approach (at least, in the form it is used in [7]) does not allow considerations of non-compactly supported functions. Thus, the validity of the theorem for arbitrarily fast decaying, but not compactly supported, functions is still not established, although it most certainly holds. On the other hand, the geometric part does not work that well in dimensions larger than 2. Development of new approaches is apparently needed in order to overcome these hurdles. A much simpler PDE approach has emerged recently [38] (see also [12] and the next section), although its achievements have been limited so far.

8.2.2 *Some open problems concerning uniqueness*

As already mentioned, one can consider the practical problems about uniqueness resolved. However, the mathematical understanding of the uniqueness problem for the restricted spherical mean operators R_S is still unsatisfactory. Here are some questions that still await their resolution:

(1) Describe uniqueness sets in dimensions larger than 2 (prove Conjecture 4). Recent limited progress as well as variations on this theme can be found in [1–12].

https://doi.org/10.1017/S0956792508007353 Published online by Cambridge University Press

(2) Prove Theorem 3 without using microlocal and harmonic polynomial tools.

(3) Prove Theorem 3 on uniqueness sets S under the condition of sufficiently fast decay (rather than compactness of support) of the function. Very little is known for the case of functions without compact support. The main known result is of [3], which describes for which values of $1 \leqslant p \leqslant \infty$ the result of Corollary 2 holds for $f \in L^p$:

Theorem 12 [3] *Let S be the boundary of a bounded domain in $\mathbb{R}^d$ and $f \in L^p(\mathbb{R}^d)$ such that $R_S f \equiv 0$. If $p \leqslant 2d/(d-1)$, then $f \equiv 0$ (and thus S is injectivity set for this space). This fails for any $p > 2d/(d-1)$.*

8.3 Inversion

Although closed form (backprojection type) inversion formulas are available now for the cases of S being a plane (and object on one side from it), a cylinder and a sphere, there is still some mystery surrounding this issue.

(1) Can one write a backprojection-type inversion formula in the case of the constant sound speed for a closed surface S which is not a sphere? We suspect that the answer to this question is negative (see also related discussion in [15, 31]).

(2) The inversion formulas for S being a sphere assume that the object to be imaged is inside S. One can check on simplest examples that if the support of the function $f(x)$ reaches outside S, the inversion formulas do not reconstruct the function correctly even inside of S. See [5, 46] for a discussion. Do backprojection-type formulas exist that do not have this deficiency?

(3) I. Gelfand's school of integral geometry has developed a marvellous machinery of the so-called κ operator, which provides a general approach to inversion and range descriptions for transforms of Radon type [43, 44]. In particular, it has been applied to the case of integration of various collections ('complexes') of spheres in [44, 47]. This consideration seems to suggest that one should not expect explicit closed form inversion formulas for R_S, even when S is a sphere. We, however, know that such formulas have been discovered [38, 77]. This apparent controversy has not been resolved.

(4) Can one derive any more explicit analytic formulas from (5.20)?

(5) Can the series expansion formulas of Theorem 8 be efficiently implemented?

It has been suggested [15, 26] to use in the TAT problem not only the values of the pressure measured by transducers on the observation surface S, but its normal derivative to S as well. If one knows both, then taking Fourier transform in the time variable and using the whole space Green's function for the Helmholtz equation leads immediately to a reconstruction formula for the solution (which seems to be much simpler than what is proposed in [26]). The problem is that this normal derivative is not measured by TAT devices. Under some circumstances (e.g., when there are no sources of ultrasound outside S), one can prove the theoretical possibility of recovering the missing normal derivative. In rare cases (planar, cylindrical or spherical surface S), when involvement of the normal derivative can be eliminated (e.g., [15, 31]), this might lead to feasible inversion algorithms,

https://doi.org/10.1017/S0956792508007353 Published online by Cambridge University Press

but in these cases, explicit and nicely implementable analytic inversion formulas are already available. So, jury is still out on the issue of plausibility of this procedure.

8.4 Stability

Stability of inversion when S is a sphere surrounding the support of $f(x)$ is the same as for the standard Radon transform, as the results of [100] and the second statement of Theorem 11 show. However, if the support reaches outside, although Corollary 2 still guarantees uniqueness of reconstruction, stability (at least for the parts outside S) is gone. Indeed, Theorem 9 shows that some parts of singularities of f outside S will not be stably 'visible.'

8.5 Range

As Theorem 9 states, the range conditions 2 and 3 of Theorem 10 are necessary also for non-spherical closed surfaces S and for functions with support outside S. They, however, are not expected to be sufficient, since Theorem 9 indicates that one might expect non-closed ranges in some cases. The same applies for non-constant sound speed case.

8.6 Sound speed recovery

A question that has started attracting attention recently is the one of simultaneous recovery from TAT data of the sound speed $c(x)$ and the object f. Clearly, one needs to worry about the recovery of the speed first. Only first steps in this direction have been taken. For instance, in [136], the problem is treated numerically with encouraging results. However, even the question of whether the sound speed is uniquely determined by TAT data has not been resolved. So far, it is known that if the speed is constant and f is supported strictly inside S, the speed is uniquely determined by the measured data [46]. It seems reasonable to try to use the range conditions of Theorem 10 to recover the sound speed. These conditions contain information of two types: the support conditions and an infinite series of orthogonality conditions. One wonders whether the orthogonality conditions help with the recovery of the speed. Although we do not know the complete answer to this question, even for constant speed the situation is not trivial. One can show that orthogonality conditions alone (without support conditions) do not uniquely determine the constant sound speed [46]. On the other hand, there is some kind of local uniqueness [46].

8.7 Attenuation effects

In all the models discussed so far in this article, attenuation of ultrasound has been neglected. It seems that this important TAT feature has not yet been sufficiently studied. See [22, 83, 114] for this issue and additional references.

Acknowledgements

The work of the first author was partially supported by the NSF DMS grants 0604778 and 0648786. The second author was partially supported by the DOE grant DE-FG02-03ER25577 and NSF DMS grant 0312292. Part of this work was completed when the

first author was at the Isaac Newton Institute for Mathematical Sciences. The authors express their gratitude to the NSF, DOE and INI for this support. The authors thank M. Agranovsky for useful discussions, M. Anastasio, G. Beylkin, P. Burgholzer, D. Finch, M. Klibanov, G. Paltauf, and P. Stefanov for providing preprints and references, and the reviewers and editors for very helpful remarks.

References

[1] Agranovsky, M. (1997) Radon transform on polynomial level sets and related problems. *Israel Math. Conf. Proc.* **11**, 1–21.

[2] Agranovsky, M. (2000) On a problem of injectivity for the Radon transform on a paraboloid. Analysis, geometry, number theory: The mathematics of Leon Ehrenpreis In: *Contemp. Math.* 251, AMS, Providence, RI, pp. 1–14.

[3] Agranovsky, M., Berenstein, C. & Kuchment, P. (1996) Approximation by spherical waves in L^p-spaces. *J. Geom. Anal.* **6**(3), 365–383.

[4] Agranovsky, M. & Kuchment, P. (2007) Uniqueness of reconstruction and an inversion procedure for thermoacoustic and photoacoustic tomography with variable sound speed. *Inv. Prob.* **23**, 2089–2102.

[5] Agranovsky, M., Kuchment, P. & Kunyansky, L. (2007) On reconstruction formulas and algorithms for the thermoacoustic and photoacoustic tomography. To appear in [125].

[6] Agranovsky, M., Kuchment, P. & Quinto, E. T. (2007) Range descriptions for the spherical mean Radon transform. *J. Funct. Anal.* **248**, 344–386.

[7] Agranovsky, M. & Quinto, E. T. (1996) Injectivity sets for the Radon transform over circles and complete systems of radial functions. *J Funct. Anal.* **139**, 383–414.

[8] Agranovsky, M. & Quinto, E. T. (2001) Geometry of stationary sets for the wave equation in $\mathbb{R}^n$: The case of finitely suported initial data. *Duke Math. J.* **107**(1), 57–84.

[9] Agranovsky, M. & Quinto, E. T. (2003) Stationary sets for the wave equation in crystallographic domains. *Trans. AMS* **355**(6), 2439–2451.

[10] Agranovsky, M. & Quinto, E. T. (2006) Remarks on stationary sets for the wave equation. *Integral Geom. Tomography, Contemp. Math.* **405**, 1–11.

[11] Agranovsky, M., Volchkov, V. V. & Zalcman, L. (1999) Conical uniqueness sets for the spherical Radon transform. *Bull. London Math. Soc.* **31**(4), 363–372.

[12] Ambartsoumian, G. & Kuchment, P. (2005) On the injectivity of the circular Radon transform. *Inv. Prob.* **21**, 473–485.

[13] Ambartsoumian, G. & Kuchment, P. (2006) A range description for the planar circular Radon transform. *SIAM J. Math. Anal.* **38**(2), 681–692.

[14] Ambartsoumian, G. & Patch, S. (2007) Thermoacoustic tomography: Numerical results. In: Alexander A. Oraevsky, Lihong V. Wang (editors) *Proceedings of SPIE 6437, Photons Plus Ultrasound: Imaging and Sensing 2007: The Eighth Conference on Biomedical Thermoacoustics, Optoacoustics, and Acousto-optics*, p. 64371B, SPIE-International Society for Optical Engine, Bellingham, Washington.

[15] Anastasio, M. A., Zhang, J., Modgil, D. & Rivière, P. J. (2007) Application of inverse source concepts to photoacoustic tomography, *Inv. Prob.* **23**, S21–S35.

[16] Anastasio, M., Zhang, J., Pan, X., Zou, Y., Ku, G. & Wang, L. V. (2005) Half-time image reconstruction in thermoacoustic tomography. *IEEE Trans. Med. Imaging* **24**, 199–210.

[17] Anastasio, M. A., Zhang, J., Sidky, E. Y., Yu Zou, Dan Xia & Xiaochuan. (2005). Feasibility of half-data image reconstruction in 3D reflectivity tomography with a spherical aperture, *IEEE Trans. Med. Imaging* **24**(9), 1100–1112.

[18] Andersson, L.-E. (1988) On the determination of a function from spherical averages. *SIAM J. Math. Anal.* **19**(1), 214–232.

[19] Andreev, V. G., Popov, D. A., Sushko, D. V., Karabutov, A. A. & Oraevsky, A. A. (2002) Image reconstruction in 3D optoacoustic tomography system with hemispherical transducer array. In: *Proc. SPIE* 4618, p. 1605-7422/02.

[20] Asgeirsson, L. (1937) Über eine Mittelwerteigenschaft von Lösungen homogener linearer partieller Differentialgleichungen zweiter Ordnung mit konstanten Koeffizienten. *Ann. Math.* **113**, 321–346.

[21] Beylkin, G. (1984) The inversion problem and applications of the generalized Radon transform. *Comm. Pure Appl. Math.* **37**, 579–599.

[22] Burgholzer, P., Grün, H., Haltmeier, M., Nuster, R. & Paltauf, G. (2007) Compensation of acoustic attenuation for high-resolution photoacoustic imaging with line detectors using time reversal. In: *Proceedings SPIE number 6437.75 Photonics West, BIOS 2007*, San Jose, CA.

[23] Burgholzer, P., Hofer, C., Matt, G. J., Paltauf, G., Haltmeier, M. & Scherzer, O. (2006) Thermoacoustic tomography using a fiber-based Fabry-Perot interferometer as an integrating line detector. In: *Proc. SPIE* 6086, pp. 434–442.

[24] Burgholzer, P., Hofer, C., Paltauf, G., Haltmeier, M. & Scherzer, O. (2005) Thermoacoustic tomography with integrating area and line detectors. *IEEE Trans. Ultrasonics, Ferroelectrics, Frequency Control* **52**(9), 1577–1583.

[25] Burgholzer, P., Matt, G., Haltmeier, M. & Patlauf, G. (2007) Exact and approximate imaging methods for photoacoustic tomography using an arbitrary detection surface. *Phys. Rev. E* **75**, 046706.

[26] Clason, C. & Klibanov, M. (2007) The quasi-reversibility method in thermoacoustic tomography in a heterogeneous medium. *SIAM J. Sci. Comput.* **30**, 1–23.

[27] Copland, J. A. et al. (2004) Bioconjugated gold nanoparticles as a molecular based contrast agent: Implications for imaging of deep tumors using optoacoustic tomography. *Mol. Imaging Biol.* **6**(5), 341–349.

[28] Courant, R. & Hilbert, D. (1962) *Methods of Mathematical Physics, Vol. II: Partial Differential Equations*, Interscience, New York.

[29] Cox, B. T., Arridge, S. R. & Beard, P. C. (2007). Photoacoustic tomography with a limited-aperture planar sensor and a reverberant cavity. *Inv. Prob.* **23**, S95–S112.

[30] Denisjuk, A. (1999) Integral geometry on the family of semi-spheres. *Fract. Calc. Appl. Anal.* **2**(1), 31–46.

[31] Devaney, A. J. & Beylkin, G. (1984) Diffraction tomography using arbitrary transmitter and receiver surfaces. *Ultrasonic Imaging* **6**, 181–193.

[32] Diebold, G. J., Sun, T. & Khan, M. I. (1991) Photoacoustic monopole radiation in one, two, and three dimensions. *Phys. Rev. Lett.* **67**(24), 3384–3387.

[33] Egorov, Yu. V. & Shubin, M. A. (1992) *Partial Differential Equations I. Encyclopaedia of Mathematical Sciences*, Springer-Verlag, Berlin, 30, 1–259.

[34] Ehrenpreis, L. (2003) *The Universality of the Radon Transform*, Oxford University Press, Oxford.

[35] Fawcett, J. A. (1985) Inversion of n-dimensional spherical averages. *SIAM J. Appl. Math.* **45**(2), 336–341.

[36] Finch, D. V. (2005) On a thermoacoustic transform. In: *Proc. Fully 3D Reconstruction Radiology Nuclear Medicine*, Salt Lake City, 5–9 July 2005. Available online at http://www.ucair.med.utah.edu/3D05/PaperPDF/3D05proceedingspart4- pages143-202.pdf

[37] Finch, D., Haltmeier, M. & Rakesh (2007) Inversion of spherical means and the wave equation in even dimensions. *SIAM J. Appl. Math.* **68**(2), 392–412.

[38] Finch, D., Patch, S. & Rakesh (2004) Determining a function from its mean values over a family of spheres. *SIAM J. Math. Anal.* **35**(5), 1213–1240.

[39] Finch, D. & Rakesh (2006) The range of the spherical mean value operator for functions supported in a ball. *Inv. Prob.* **22**, 923–938.

[40] Finch, D. & Rakesh (2007) Recovering a function from its spherical mean values in two and three dimensions. To appear in [125].

[41] Finch, D. & Rakesh (2007) The spherical mean value operator with centers on a sphere. *Inv. Prob.* **23**(6), S37–S50.
[42] Flatto, L., Newman, D. J. & Shapiro, H. S. (1966) The level curves of harmonic functions. *Trans. Amer. Math. Soc.* **123**, 425–436.
[43] Gelfand, I., Gindikin, S. & Graev M. (1980) Integral geometry in affine and projective spaces. *J. Sov. Math.* **18**, 39–167.
[44] Gelfand, I., Gindikin, S. & Graev M. (2003) *Selected Topics in Integral Geometry. Transl. Math. Monogr.* vol. 220, AMS, Providence, RI.
[45] Gelfand, I., Graev M. & Vilenknin, N. (1965) *Generalized Functions, vol. 5: Integral Geometry and Representation Theory*, Academic Press, New York.
[46] Georgieva-Hristova, Y., Kuchment, P. & Nguyen, L. (2007) On reconstruction and time reversal in thermoacoustic tomography, preprint.
[47] Gindikin, S. (1995) Integral geometry on real quadrics. In: *Lie groups and Lie algebras: E. B. Dynkin's Seminar*, Amer. Math. Soc. Transl. Ser. 2, 169, AMS, Providence, RI, pp. 23–31.
[48] Greenleaf, A. & Uhlmann, G. (1990) Microlocal techniques in integral geometry. *Contemp. Math.* **113**, 149–155.
[49] Grün, H., Haltmeier, M., Paltauf, G. & Burgholzer, P. (2007) Photoacoustic tomography using a fiber based Fabry-Perot interferometer as an integrating line detector and image reconstruction by model-based time reversal method. In: *Proc. SPIE*, 6631, p. 663107.
[50] Guillemin, V. (1975) Fourier integral operators from the Radon transform point of view. *Proc. Symposia Pure Math.* **27**, 297–300.
[51] Guillemin, V. (1985) On some results of Gelfand in integral geometry. *Proc. Symposia Pure Math.* **43**, 149–155.
[52] Guillemin, V. & Sternberg S. (1977) *Geometric Asymptotics.* AMS, Providence, RI.
[53] Gusev, V. E. & Karabutov, A. A. (1993) *Laser Optoacoustics*, American Institute of Physics, New York.
[54] Haltmeier, M., Burgholzer, P., Hofer, C., Paltauf, G., Nuster, R. & Scherzer, O. (2005) Thermoacoustic tomography using integrating line detectors. *Ultrasonics Symp.* **1**, 166–169.
[55] Haltmeier, M., Burgholzer, P., Paltauf, G. & Scherzer, O. (2004) Thermoacoustic computed tomography with large planar receivers. *Inv. Prob.* **20**, 1663–1673.
[56] Haltmeier, M. & Fidler, T. Mathematical challenges arising in thermoacoustic tomography with line detectors, preprint arXiv:math.AP/0610155.
[57] Haltmeier, M., Paltauf, G., Burgholzer, P. & Scherzer, O. (2005) Thermoacoustic tomography with integrating line detectors. In: *Proc. SPIE* 5864, p. 586402-8.
[58] Haltmeier, M., Scherzer, O., Burgholzer, P. & Paltauf, G. (2005) Thermoacoustic computed tomography with large planar receivers. *ECMI Newslett.* **37**, 31–34. http://www.it.lut.fi/mat/EcmiNL/ecmi37/
[59] Haltmeier, M., Schuster, T. & O. Scherzer (2005) Filtered backprojection for thermoacoustic computed tomography in spherical geometry. *Math. Methods Appl. Sci.* **28**, 1919–1937.
[60] Helgason, S. (1980) *The Radon Transform*, Birkhäuser, Basel.
[61] Helgason, S. (2000) *Groups and Geometric Analysis*, AMS, Providence, RI.
[62] Herman, G. (editor) (1979) *Topics in Applied Physics, Vol. 32*: *Image Reconstruction from Projections* Springer-Verlag, Berlin.
[63] Hörmander, L. (1983) *The Analysis of Linear Partial Differential Operators*, Vol. 1, Springer-Verlag, New York.
[64] *Inverse Problems* (2007) (a special issue devoted to thermoacoustic tomography) **23**(6).
[65] Jin, X. & Wang, L. V. (2006) Thermoacoustic tomography with correction for acoustic speed variations. *Phy. Med. Biol.* **51**, 6437–6448.
[66] John, F. (1971) *Plane Waves and Spherical Means Applied to Partial Differential Equations*, Dover, New York.
[67] Kak, A. C. & Slaney, M. (2001) *Principles of Computerized Tomographic Imaging*, SIAM, Philadelphia, PA.

[68] Köstli K. P., Frenz, M., Bebie, H. & Weber H. P. (2001) Temporal backward projection of optoacoustic pressure transients using Fourier transform methods. *Phys. Med. Biol.* **46**, 1863–1872

[69] Kruger, R. A., Kiser, W. L., Reinecke, D. R. & Kruger, G. A. (2003) Thermoacoustic computed tomography using a conventional linear transducer array. *Med. Phys.* **30**(5), 856–860.

[70] Kruger, R. A., Liu. P., Fang, Y. R. & Appledorn, C. R. (1995) Photoacoustic ultrasound (PAUS) reconstruction tomography. *Med. Phys.* **22**, 1605–1609.

[71] Kuchment, P. (1993), unpublished.

[72] Kuchment, P. (2006) Generalized transforms of radon type and their applications. In: *American Mathematical Society Short Course*, 3–4 January 2005, Atlanta, GA, *Proc. Symp. Appl. Math.* vol. 63, AMS, Providence RI, pp. 67–91.

[73] Kuchment, P., Lancaster, K. & Mogilevskaya, L. (1995) On local tomography. *Inv. Prob.* **11**, 571–589.

[74] Kuchment, P. & Lvin S. (1990) Paley-Wiener theorem for the exponential Radon transform. *Acta Applicandae Mathematicae* (18), 251–260.

[75] Kuchment, P. & Lvin S. (1991) The range of the exponential radon transform. *Sov. Math. Dokl.* **42**(1), 183–184.

[76] Kuchment, P. & Quinto, E. T. (2003). Some problems of integral geometry arising in tomography. In: *The University of the Radon Transform*, Oxform University Press, Oxford, Capter XI.

[77] Kunyansky, L. (2007) Explicit inversion formulae for the spherical mean Radon transform. *Inv. Prob.* **23**, 737–783.

[78] Kunyansky, L. (2007) A series solution and a fast algorithm for the inversion of the spherical mean Radon transform. *Inv. Prob.* **23**, S11–S20.

[79] Lin, V. & Pinkus, A. (1993) Fundamentality of ridge functions. *J. Approx. Theory* **75**, 295–311.

[80] Lin, V. & Pinkus, A (1994) Approximation of multivariate functions. In H. P. Dikshit & C. A. Micchelli (editors), *Advances in Computational Mathematics*, World Scientific, pp. 1–9.

[81] Louis, A. K. & Quinto, E. T. (2000) Local tomographic methods in Sonar. In *Surveys on Solution Methods for Inverse Problems*, Springer, Vienna, David Colton, Heinz W. Engl, Alfred K. Louis, and Joyce R. McLaughlin, pp. 147–154.

[82] Lvin S. (1994) Data correction and restoration in emission tomography. In E. T. Quinto, M. Cheney & P. Kuchment (editors), *Tomography, Impedance Imaging, and Integral Geometry*, Lectures in Appl. Math., Vol. 30, AMS, Providence, RI, pp. 149–155.

[83] Maslov, K., Zhang, H. F. & Wang, L. V. (2007) Effects of wavelength-dependent fluence attenuation on the noninvasive photoacoustic imaging of hemoglobin oxygen saturation in subcutaneous vasculature in vivo. *Inv. Prob.* **23**, S113–S122.

[84] *Mathematics and Physics of Emerging Biomedical Imaging*, The National Academies Press, 1996. Available online at http://www.nap.edu/catalog.php?record_id=5066#toc.

[85] Natterer, F. (1986) *The Mathematics of Computerized Tomography*, Wiley, New York.

[86] Natterer, F. & Wübbeling, F. (2001) *Mathematical Methods in Image Reconstruction*, Monographs on Mathematical Modeling and Computation **5**, SIAM, Philadelphia, PA.

[87] Nessibi, M. M., Rachdi, L. T. & Trimeche, K. (1995) Ranges and inversion formulas for spherical mean operator and its dual. *J. Math. Anal. Appl.* **196**(3), 861–884.

[88] Niederhauser, J. J., Jaeger, M., Lemor, R., Weber, P. & Frenz, M. (2005) Combined ultrasound and optoacoustic system for real-time high-contrast vascular imaging *in vivo*. *IEEE Trans. Med. Imaging* **24**, 436–440.

[89] Nilsson, S. (1997) *Application of Fast Backprojection Techniques for Some Inverse Problems of Integral Geometry*. Linkoeping studies in science and technology, Dissertation 499, Department of Mathematics, Linkoeping University, Linkoeping, Sweden.

[90] Nolan, C. J. & Cheney, M. (2002) Synthetic aperture inversion. *Inv. Prob.* **18**, 221–235.

[91] Norton, S. J. (1980) Reconstruction of a two-dimensional reflecting medium over a circular domain: Exact solution. *J. Acoust. Soc. Am.* **67**, 1266–1273.

[92] Norton, S. J. & Linzer, M. (1981) Ultrasonic reflectivity imaging in three dimensions: Exact inverse scattering solutions for plane, cylindrical, and spherical apertures. *IEEE Trans. Biomed. Eng.*, **28**, 200–202.
[93] Novikov, R. (2002) On the range characterization for the two-dimensional attenuated X-ray transform. *Inv. Prob.* **18**, 677–700.
[94] Olafsson, G. & Quinto, E. T. (editors), (2006) The Radon transform, inverse problems, and tomography. In: *American Mathematical Society Short Course* 3–4 January 2005, Atlanta, GA, *Proc. Symp. Appl. Math.* vol. 63, AMS, Providence, RI.
[95] Oraevsky, A. A., Esenaliev, R. O., Jacques, S. L. Tittel, F. K. (1996) Laser optoacoustic tomography for medical diagnostics principles. In: *Proc. SPIE* 2676, p. 22.
[96] Oraevsky, A. A. & Karabutov, A. A. (2002) Time-Resolved Detection of Optoacoustic Profiles for Measurement of Optical Energy Distribution in Tissues. In: V. V. Tuchin (editors), *Handbook of Optical Biomedical Diagonstics*, SPIE, Bellingham, WA, Chapter 10.
[97] Oraevsky A. A. & Karabutov, A. A. (2003) Optoacoustic tomography. In: T. Vo-Dinh (editors), *Biomedical Photonics Handbook*, CRC Press, Boca Raton, FL, Chapter 34, **34**-1–**34**-34.
[98] Palamodov, V. P. (2000) Reconstruction from limited data of arc means. *J. Fourier Anal. Appl.* **6**(1), 25–42.
[99] Palamodov, V. P. (2004) *Reconstructive Integral Geometry*, Birkhäuser, Basel.
[100] Palamodov, V. (2007) Remarks on the general Funk-Radon transform and thermoacoustic tomography. Preprint arxiv: math.AP/0701204.
[101] Paltauf, G., Burgholzer, P., Haltmeier, M. & Scherzer, O. (2005) Thermoacoustic tomography using optical line detection. In: *Proc. SPIE* 5864, pp. 7–14.
[102] Paltauf, G., Nuster, R., Haltmeier, M. & Burgholzer, P. (2007) Thermoacoustic Computed Tomography using a Mach-Zehnder interferometer as acoustic line detector. *Appl. Opt.* **46**(16), 3352–3358.
[103] Passechnik, V. I., Anosov, A. A. & Bograchev, K. M. (2000) Fundamentals and prospects of passive thermoacoustic tomography. *Crit. Rev. Biomed. Eng.* **28**(3&4), 603–640.
[104] Patch, S. K. (2004) Thermoacoustic tomography – Consistency conditions and the partial scan problem. *Phys. Med. Biol.* **49**, 1–11.
[105] Patch, S. K. & Scherzer, O. (2007) Photo- and thermo-acoustic imaging (Guest Editors. Introduction). *Inv. Prob.* **23**, S01–S10.
[106] Popov D. A. & Sushko, D. V. (2002) A parametrix for the problem of optical-acoustic tomography. *Dokl. Math.* **65**(1), 19–21.
[107] Popov D. A. & Sushko, D. V. (2004) Image restoration in optical-acoustic tomography. *Prob. Information Transmission* **40**(3), 254–278.
[108] Quinto, E. T. (1980) The dependence of the generalized Radon transform on defining measures. *Trans. Amer. Math. Soc.* **257**, 331–346.
[109] Quinto, E. T. (1993) Singularities of the X-ray transform and limited data tomography in $\mathbb{R}^2$ and $\mathbb{R}^3$. *SIAM J. Math. Anal.* **24**, 1215–1225.
[110] Quinto, E. T. (2006) An introduction to X-ray tomography and Radon transforms. In: *American Mathematical Society Short Course*, 3–4 January 2005, Atlanta, GA, *Proc. Symp. Appl. Math.* vol. 63, AMS, Providence RI, pp. 1–23.
[111] Ramm, A. G. (1985) Inversion of the backscattering data and a problem of integral geometry. *Phys. Lett. A* **113**(4), 172–176.
[112] Ramm, A. G. (2002) Injectivity of the spherical means operator. *C. R. Math. Acad. Sci. Paris* **335**(12), 1033–1038.
[113] Ramm, A. G. & Zaslavsky, A. I. (1993) Reconstructing singularities of a function from its Radon transform. *Math. Comput. Modelling* **18**(1), 109–138.
[114] La Rivière, P. J., Zhang, J. & Anastasio, M. A. (2006) *Opt. Lett.* **31**(6), 781–783.
[115] Romanov, V. G. (1967) Reconstructing functions from integrals over a family of curves. *Sib. Mat. Zh.* **7**, 1206–1208.

[116] Schuster, T. & Quinto, E. T. (2005) On a regularization scheme for linear operators in distribution spaces with an application to the spherical Radon transform. *SIAM J. Appl. Math.* **65**(4), 1369–1387.
[117] Stefanov, P. & Uhlmann, G. (2008) Integral geometry of tensor fields on a class of non-simple Riemannian manifolds. *Am. J. Math.* **130**(1), 239–268.
[118] Strichartz, R. S. (2003) *A Guide to Distribution Theory and Fourier Transforms*, World Scientific, Singapore; River Edge, NJ.
[119] Tam, A. C. (1986) Applications of photoacoustic sensing techniques. *Rev. Mod. Phys.* **58**(2), 381–431.
[120] Tataru, D. (1995) Unique continuation for solutions to PDEs; between Hörmander's theorem and Holmgren's theorem. *Comm. PDE* **20**, 814–822.
[121] Tuchin, V. V. (editor) (2002) *Handbook of Optical Biomedical Diagnostics*, SPIE, Bellingham, WA.
[122] Vainberg, B. (1975) The short-wave asymptotic behavior of the solutions of stationary problems, and the asymptotic behavior as $t \to \infty$ of the solutions of nonstationary problems. *Russian Math. Surveys* **30**(2), 1–58.
[123] Vainberg, B. (1982). *Asymptotics Methods in the Equations of Mathematical Physics*, Gordon & Breach, New York–London.
[124] Vo-Dinh, T. (editor) (2003) *Biomedical Photonics Handbook*. CRC Press, Boca Raton, FL.
[125] Wang, L. (editor) *Photoacoustic Imaging and Spectroscopy*, CRC Press, Boca Raton, FL, to appear.
[126] Wang, L. V. & Wu, H. (2007) *Biomedical Optics. Principles and Imaging*. Wiley-Interscience, Hoboken, New Jersey.
[127] Wang, L. H. V. & Yang, X. M. (2007) Boundary conditions in photoacoustic tomography and image reconstruction. *J. Biomed. Opt.* **12**(1), 10.
[128] Wang, X., Pang, Y., Ku, G., Xie, X., Stoica, G. & Wang, L. (2003) Noninvasive laser-induced photoacoustic tomography for structural and functional *in vivo* imaging of the brain. *Nat. Biotechnol.* **21**(7), 803–806.
[129] Xu, M. & Wang, L.-H. V. (2002) Time-domain reconstruction for thermoacoustic tomography in a spherical geometry. *IEEE Trans. Med. Imaging* **21**, 814–822.
[130] Xu, M. & Wang, L.-H. V. (2005) Universal back-projection algorithm for photoacoustic computed tomography. *Phys. Rev. E* **71**, 016706.
[131] Xu, M. & Wang, L.-H. V. (2006) Photoacoustic imaging in biomedicine. *Rev. Sci. Instrum.* **77**, 041101-01–041101-22.
[132] Xu, Y., Feng, D. & Wang, L.-H. V. (2002) Exact frequency-domain reconstruction for thermoacoustic tomography: I. Planar geometry. *IEEE Trans. Med. Imaging* **21**, 823–828.
[133] Xu, Y., Xu, M. & Wang, L.-H. V. (2002) Exact frequency-domain reconstruction for thermoacoustic tomography: II. Cylindrical geometry. *IEEE Trans. Med. Imaging* **21**, 829–833.
[134] Xu, Y., Wang, L., Ambartsoumian, G. & Kuchment, P. (2004) Reconstructions in limited view thermoacoustic tomography. *Med. Phys.* **31**(4), 724–733.
[135] Xu, Y., Wang, L., Ambartsoumian, G. & Kuchment, P. (2007) Limited view thermoacoustic tomography. To appear in [126].
[136] Zhang, J. & Anastasio, M. A. (2006) Reconstruction of speed-of-sound and electromagnetic absorption distributions in photoacoustic tomography. In: *Proc. SPIE* 6086, p. 608619.
[137] Zobin, N. (1993). Unpublished.